Modern Physics Letters B
2150486 (16 pages)

DOI: 10.1142/s0217984921504868

Magnetic properties and phase diagrams of the mixed spin-$(\frac{1}{2}, \frac{3}{2})$ Ising–Heisenberg model in the mean field approximation

G. Seto*, R. A. A. Yessoufou*,†, A. Kpadonou‡, E. Albayrak§,¶ and F. Hontinfinde*,†

*Institute of Mathematic and Physical Sciences (IMSP), Benin
†Department of Physics, University of Abomey-Calavi, Republic of Benin
‡ENS and Laboratory of Physics and Applications (LPA), d'Abomey, Benin
§Department of Physics, Erciyes University, Kayseri 38039, Turkey
¶albayrak@erciyes.edu.tr

Received 2 June 2021
Revised 15 July 2021
Accepted 10 August 2021
Published 24 September 2021

In this paper, the effects of the longitudinal D_z and the transverse D_x crystal fields on the mixed spin-$(\frac{1}{2}, \frac{3}{2})$ Ising–Heisenberg model have been studied. The thermodynamic properties of the model are obtained by using a new approach of the mean field approximation (MFA). The thermal variations of the order-parameters and the total magnetic susceptibility of the model are carefully investigated to obtain the phase diagrams on the $(D_x/J, k_BT/J)$ planes for $z = 3$ and on the $(D_z/J, k_BT/J)$ planes for $z = 3, 4$ and 6. The existence of compensation temperatures between the sublattice magnetizations, $T_{\mathrm{comp},M}$, and the two components of the quadrupole moments, $T_{\mathrm{comp},Q}$, are observed. Our results are compared with other existing works in the literature and reliable agreements are found.

Keywords: Transverse crystal field; longitudinal crystal field; compensation; mean field; mixed spin.

PACS Number(s): 61.10.Nz, 61.66.Fn, 75.40.Gb

1. Introduction

The mixed-spin models with various kinds of spins have been studied extensively, because they have less translational symmetry than their single counterparts and may show many new phenomena, such as the compensation behavior, that cannot be observed in the single-spin Ising models. These models are well adopted to study a certain type of ferrimagnetism which is of great interest because of its interesting and possible useful properties. Experimentally, it was shown that the

¶Corresponding author.

MnNi (EDTA)6H2O complex is a mixed-spin system[1] and there is also evidence for the mixed spin-1/2 and spin-3/2 system, i.e. amorphous V(TCNE)$x \cdot y$ solvent, in which TCNE is a tetracyanoethylene, is an organometallic compound seems to have this mixed-spin structure which was found to stay in ferrimagnetic ordering until 400 K's.[2]

In addition, Heisenberg's model continues to be of great interest for theoretical researches because it offers the possibility of studying the quantum phase transitions. One of the difficulties linked to this model is the non-commutativity of the spin operators which leads to uncertainty in the measurements of the observables. To get around this difficulty, one can resort to hybrid classical-quantum models which constitute both Ising and as well as Heisenberg spins models.[3] Several studies have been performed on the mixed-spin Ising–Heisenberg or its modified versions.[4–10] In most of these works, only the longitudinal crystal field (LCF) component D_z has been considered in their Hamiltonian's model. Since it has been proven that the transverse component also influences the critical behaviors of the system, several other works have also looked into this aspect. The critical behaviors of a mixed spin-$(\frac{1}{2}, s_B)$ Ising system with transverse crystal field (TCF) D_x,[11] the magnetic properties of a bond-diluted mixed spin-$(\frac{1}{2}, 1)$ Ising model with uniaxial and biaxial single-ion anisotropy,[12] the magnetic properties of a multilayer system consisting of L-layers of spin-$\frac{1}{2}$ atoms and L-layers of spin-1 atoms with disordered interface,[13] the effect of TCF on ferromagnetic (FM) or ferrimagnetic (FI) mixed spin-$\frac{1}{2}$ and spin-1 (spin-3/2) Ising bilayer system,[14] the FM or FI bilayer system consisting of different monolayers with spin-$\frac{1}{2}$ and spin-1 (spin-$\frac{3}{2}$),[15] the critical behaviors of a TCF and a bimodal magnetic field mixed spin Ising model with bond dilution or bond percolation threshold,[16] compensation behaviors of mixed Ising model with a TCF in an external magnetic field,[17] the alternating-bond mixed spin-$(\frac{1}{2}, 1)$ Ising chain with both LCF and TCF are a few examples.[18] In addition, the effects of an LCF and a TCF on the mixed spin-$(1, \frac{1}{2})$ Ising–Heisenberg model were examined on a honeycomb lattice by using a new approach in the MFA.[19]

There are also a few works which consider the magnetic properties of the mixed spin-$(\frac{1}{2}, \frac{3}{2})$ with LCF as follows. The Glauber-type stochastic dynamics was used to describe the time evolution of the two interpenetrating square sublattices having mixed-spins 1/2 and 3/2 with a crystal-field interaction in the presence of a time-dependent oscillating external magnetic field within a MFA.[20] The investigation of the diluted model on a honeycomb lattice within the effective-field theory (EFT) has exhibited two compensation points.[21] Again using the EFT, the study of the model has led to a variety of interesting phenomena in phase diagrams due to the influence of the LCF.[22] The thermal behaviors of the order-parameters and phase diagrams of the Ising model were also investigated within the EFT.[23] The model was studied by using the Monte Carlo (MC) simulation on a square lattice and it was found that the compensation temperatures depends extremely on the interactions in the Hamiltonian.[24] By using Green's function method, the effects of the nearest- and

next-nearest-neighbor interactions between the spins on the magnetic behavior of quantum Heisenberg system were examined.[25] It should be noted that this system has also been investigated on the Bethe lattice and on the two-fold Cayley tree by means of the exact recursion relations (ERR),[26,27] and also on the honeycomb lattice by using the exact star-triangle mapping transformations.[28] It is also important to note that the effects of both exchange anisotropy and single-ion anisotropy on the phase diagrams and the magnetization curves of the FM Heisenberg model were investigated by using Oguchi approximation.[29] Recently, the effects of the LCF and longitudinal magnetic field on the order-parameters of the Blume–Capel model were studied by using the ERRs on the Bethe lattice.[30]

Among all these different studies above, only Ref. 19 examined the effects of both LCF and TCF on the mixed spin-$(\frac{1}{2}, 1)$ Ising–Heisenberg model. In order to extend this study to the mixed spin models with that of half-integer spins, we now investigate the thermal variations of the order-parameters, susceptibility and the phase diagrams of the mixed spin-$(\frac{1}{2}, \frac{3}{2})$ Ising–Heisenberg model by using a new shape of the MFA where particular attention is given to the study of the compensation properties of the model.

The remaining parts of this work are constructed as follows. The formulation of the model and the details of calculations are given in Sec. 2. Section 3 contains the detailed numerical findings concerning the thermal behaviors of the order-parameters and susceptibility. Section 4 consists of the phase diagrams which are carefully exposed and discussed, and in the last section, we present a brief summary and conclusions.

2. Model and Formalism

The mixed spin-(S_A, S_B) Ising–Heisenberg model may be described by the following Hamiltonian:

$$\hat{H} = -J \sum_{\langle i,j \rangle} \hat{S}^z_{iA} \hat{S}^z_{jB} - D_z \sum_{j \in B} (\hat{S}^z_{jB})^2 - D_x \sum_{j \in B} (\hat{S}^x_{jB})^2 - h_A \sum_{i \in A} \hat{S}^z_{iA} - h_B \sum_{j \in B} \hat{S}^z_{jB}, \tag{1}$$

where $\hat{S}^\delta_{iA}$ and $\hat{S}^\delta_{jB}$ with $(\delta = x, z)$ are the components of spin-$\frac{1}{2}$ and spin-$\frac{3}{2}$ operators for the sublattices A and B, respectively. J is the FM exchange interaction between the nearest-neighbor (NN) spins S_{iA} and S_{jB}. D_x and D_z are the TCF and LCF parameters, respectively, acting only on the sites with spin-$\frac{3}{2}$. Lastly, h_A and h_B are the longitudinal external magnetic fields acting on the spins of both sublattices.

It is well known that in the ordinary MFA, the NN pair interactions between the spin components are treated exactly and the rest of interactions are replaced with the effective field terms. In this work, we consider the opposite approximation, i.e. the NN pair interactions between the spin components are approximated and the

rest of interactions are treated exactly. By using this new approach of the MFA,[19] the Hamiltonian given in Eq. (1) can be written as

$$-\beta\hat{H} = -\beta\sum_{i,j}\hat{H}^{(ij)}_{\mathrm{MFA}}, \tag{2}$$

where

$$\begin{aligned}-\beta\hat{H}^{(ij)}_{\mathrm{MFA}} &= \beta Jz(M^z_{\frac{3}{2}}\hat{S}^z_{iA} + M^z_{\frac{1}{2}}\hat{S}^z_{jB}) + \beta D_z(\hat{S}^z_{jB})^2 \\ &\quad + \beta D_x(\hat{S}^x_{jB})^2 + \beta h_A\hat{S}^z_{iA} + \beta h_B\hat{S}^z_{jB},\end{aligned} \tag{3}$$

z is the number of NN spins, $M^z_{\frac{1}{2}} = \langle\hat{S}^z_{iA}\rangle$ and $M^z_{\frac{3}{2}} = \langle\hat{S}^z_{jB}\rangle$ are the thermal averages corresponding to the sublattice magnetizations. The spin operators corresponding to spin-$\frac{1}{2}$ and spin-$\frac{3}{2}$ are given by

$$\hat{S}^z_{iA} = \frac{1}{2}\begin{pmatrix}1 & 0\\ 0 & -1\end{pmatrix}, \quad \hat{S}^z_{jB} = \frac{1}{2}\begin{pmatrix}3 & 0 & 0 & 0\\ 0 & 1 & 0 & 0\\ 0 & 0 & -1 & 0\\ 0 & 0 & 0 & -3\end{pmatrix},$$

$$\hat{S}^x_{jB} = \frac{1}{2}\begin{pmatrix}0 & \sqrt{3} & 0 & 0\\ \sqrt{3} & 0 & 2 & 0\\ 0 & 2 & 0 & \sqrt{3}\\ 0 & 0 & \sqrt{3} & 0\end{pmatrix}, \quad (\hat{S}^z_{jB})^2 = \frac{1}{4}\begin{pmatrix}9 & 0 & 0 & 0\\ 0 & 1 & 0 & 0\\ 0 & 0 & 1 & 0\\ 0 & 0 & 0 & 9\end{pmatrix},$$

$$(\hat{S}^x_{jB})^2 = \frac{1}{4}\begin{pmatrix}3 & 0 & 2\sqrt{3} & 0\\ 0 & 7 & 0 & 2\sqrt{3}\\ 2\sqrt{3} & 0 & 7 & 0\\ 0 & 2\sqrt{3} & 0 & 3\end{pmatrix}.$$

The basis vectors of spin-$\frac{1}{2}$ and spin-$\frac{3}{2}$ are defined in spaces of dimension 2 and 4, respectively. The study of the mixed spin-$\frac{1}{2}$ and spin-$\frac{3}{2}$ system must be done in a space of dimension 8. Thus, we use the direct product with unitary matrix $\mathbf{I_{2\times 2}}$ and $\mathbf{I_{4\times 4}}$ which are written as

$$\mathbf{I_{2\times 2}} = \begin{pmatrix}1 & 0\\ 0 & 1\end{pmatrix}, \quad \mathbf{I_{4\times 4}} = \begin{pmatrix}1 & 0 & 0 & 0\\ 0 & 1 & 0 & 0\\ 0 & 0 & 1 & 0\\ 0 & 0 & 0 & 1\end{pmatrix}.$$

Using the direct product, Eq. (3) can be rewritten as follows:

$$\begin{aligned}-\beta\hat{H}_{\mathrm{MFA}}^{(ij)} &= \beta Jz[M_{\frac{3}{2}}^{z}(I_{4\times4}\otimes\hat{S}_{iA}^{z}) + M_{\frac{1}{2}}^{z}(\hat{S}_{jB}^{z}\otimes I_{2\times2})]\\ &\quad+\beta D_z(\hat{S}_{jB}^{z})^2\otimes I_{2\times2}+\beta D_x(\hat{S}_{jB}^{x})^2\otimes I_{2\times2}\\ &\quad+\beta h_A I_{4\times4}\otimes\hat{S}_{iA}^{z}+\beta h_B\hat{S}_{jB}^{z}\otimes I_{2\times2}. \end{aligned} \tag{4}$$

Now, one can obtain the matrix representation of the operator $-\beta\hat{H}_{\mathrm{MFA}}^{(ij)}$ in the form of 8×8 matrix as

$$\begin{pmatrix}
a_{11} & 0 & 0 & 0 & \frac{\beta\sqrt{3}D_x}{2} & 0 & 0 & 0\\
0 & a_{22} & 0 & 0 & 0 & \frac{\beta\sqrt{3}D_x}{2} & 0 & 0\\
0 & 0 & a_{33} & 0 & 0 & 0 & \frac{\beta\sqrt{3}D_x}{2} & 0\\
0 & 0 & 0 & a_{44} & 0 & 0 & 0 & \frac{\beta\sqrt{3}D_x}{2}\\
\frac{\beta\sqrt{3}D_x}{2} & 0 & 0 & 0 & a_{55} & 0 & 0 & 0\\
0 & \frac{\beta\sqrt{3}D_x}{2} & 0 & 0 & 0 & a_{66} & 0 & 0\\
0 & 0 & \frac{\beta\sqrt{3}D_x}{2} & 0 & 0 & 0 & a_{77} & 0\\
0 & 0 & 0 & \frac{\beta\sqrt{3}D_x}{2} & 0 & 0 & 0 & a_{88}
\end{pmatrix},$$

where the diagonal matrix elements are given as

$$\begin{aligned}
a_{11} &= \frac{\beta JzM_{\frac{3}{2}}^{z}}{2}+3\frac{\beta JzM_{\frac{1}{2}}^{z}}{2}+3\frac{\beta D_x}{4}+9\frac{\beta D_z}{4}+\frac{\beta h_A}{2}+3\frac{\beta h_B}{2},\\
a_{22} &= -\frac{\beta JzM_{\frac{3}{2}}^{z}}{2}+3\frac{\beta JzM_{\frac{1}{2}}^{z}}{2}+3\frac{\beta D_x}{4}+9\frac{\beta D_z}{4}-\frac{\beta h_A}{2}+3\frac{\beta h_B}{2},\\
a_{33} &= \frac{\beta JzM_{\frac{3}{2}}^{z}}{2}+\frac{\beta JzM_{\frac{1}{2}}^{z}}{2}+7\frac{\beta D_x}{4}+\frac{\beta D_z}{4}+\frac{\beta h_A}{2}+\frac{\beta h_B}{2},\\
a_{44} &= -\frac{\beta JzM_{\frac{3}{2}}^{z}}{2}+\frac{\beta JzM_{\frac{1}{2}}^{z}}{2}+7\frac{\beta D_x}{4}+\frac{\beta D_z}{4}-\frac{\beta h_A}{2}+\frac{\beta h_B}{2},\\
a_{55} &= \frac{\beta JzM_{\frac{3}{2}}^{z}}{2}-\frac{\beta JzM_{\frac{1}{2}}^{z}}{2}+7\frac{\beta D_x}{4}+\frac{\beta D_z}{4}+\frac{\beta h_A}{2}-\frac{\beta h_B}{2},\\
a_{66} &= -\frac{\beta JzM_{\frac{3}{2}}^{z}}{2}-\frac{\beta JzM_{\frac{1}{2}}^{z}}{2}+7\frac{\beta D_x}{4}+9\frac{\beta D_z}{4}-\frac{\beta h_A}{2}-\frac{\beta h_B}{2},
\end{aligned}$$

$$a_{77} = \frac{\beta J z M_{\frac{3}{2}}^z}{2} - 3\frac{\beta J z M_{\frac{1}{2}}^z}{2} + 3\frac{\beta D_x}{4} + 9\frac{\beta D_z}{4} + \frac{\beta h_A}{2} - 3\frac{\beta h_B}{2},$$
$$a_{88} = -\frac{\beta J z M_{\frac{3}{2}}^z}{2} - 3\frac{\beta J z M_{\frac{1}{2}}^z}{2} + 3\frac{\beta D_x}{4} + 9\frac{\beta D_z}{4} - \frac{\beta h_A}{2} - 3\frac{\beta h_B}{2}. \quad (5)$$

The eigenvalues of this matrix are the main ingredients in calculating the thermodynamic functions and are obtained as follows:

$$\begin{aligned}
\lambda_{1,2} &= [a_{88} + a_{44} \pm \sqrt{(a_{88} - a_{44})^2 + 4a_{15}^2})/2], \\
\lambda_{3,4} &= [a_{77} + a_{33} \pm \sqrt{(a_{77} - a_{33})^2 + 4a_{15}^2})/2], \\
\lambda_{5,6} &= [a_{66} + a_{22} \pm \sqrt{(a_{66} - a_{22})^2 + 4a_{15}^2})/2], \\
\lambda_{7,8} &= [a_{55} + a_{11} \pm \sqrt{(a_{55} - a_{11})^2 + 4a_{15}^2})/2],
\end{aligned} \quad (6)$$

with

$$a_{15} = \frac{\beta\sqrt{3}D_x}{2}.$$

Since all the information in our system is contained in the partition function, it is calculated by using the formula as

$$Z = \mathrm{Tr}_{ij} \exp\left(-\beta \hat{H}_{\mathrm{MFA}}^{(ij)}\right) = \sum_{i=1}^{8} e^{-\beta\lambda_i}. \quad (7)$$

The explicit form of the partition function Z is given by

$$\begin{aligned}
Z = {} & 2\exp\left(\frac{A_1}{2}\right)\cosh\left(\frac{C}{2}\right) + 2\exp\left(\frac{A_2}{2}\right)\cosh\left(\frac{C}{2}\right) \\
& + 2\exp\left(\frac{A_3}{2}\right)\cosh\left(\frac{E}{2}\right) + 2\exp\left(\frac{A_4}{2}\right)\cosh\left(\frac{E}{2}\right),
\end{aligned} \quad (8)$$

where the coefficients C, E, A_1, A_2, A_3 and A_4 are given by

$$C = \beta\sqrt{(-D_x + 2D_z - 2h_B - 2JzM_{\frac{1}{2}}^z)^2 + 3D_x^2},$$
$$E = \beta\sqrt{(D_x - 2D_z - 2h_B - 2JzM_{\frac{1}{2}}^z)^2 + 3D_x^2},$$
$$A_1 = -\beta J z M_{3/2}^z - \beta J z M_{\frac{1}{2}}^z - \beta h_A - \beta h_B + \frac{5\beta(D_x + D_z)}{2},$$
$$A_2 = \beta J z M_{\frac{3}{2}}^z - \beta J z M_{\frac{1}{2}}^z + \beta h_A - \beta h_B + \frac{5\beta(D_x + D_z)}{2},$$
$$A_3 = -\beta J z M_{\frac{3}{2}}^z + \beta J z M_{\frac{1}{2}}^z - \beta h_A + \beta h_B + \frac{5\beta(D_x + D_z)}{2},$$
$$A_4 = \beta J z M_{\frac{3}{2}}^z + \beta J z M_{\frac{1}{2}}^z + \beta h_A + \beta h_B + \frac{5\beta(D_x + D_z)}{2}.$$

The magnetization of the sublattice A is calculated by the formula

$$M^z_{\frac{1}{2}} = \frac{1}{\beta Z}\frac{\partial Z}{\partial h_A} \tag{9}$$

and it is explicitly expressed as

$$M^z_{\frac{1}{2}} = \frac{1}{Z}\bigg[-\exp\left(\frac{A_1}{2}\right)\cosh\left(\frac{C}{2}\right)+\exp\left(\frac{A_2}{2}\right)\cosh\left(\frac{C}{2}\right) - \exp\left(\frac{A_3}{2}\right)\cosh\left(\frac{E}{2}\right)+\exp\left(\frac{A_4}{2}\right)\cosh\left(\frac{E}{2}\right)\bigg]. \tag{10}$$

For the sublattice B, one can obtain the magnetization and, transverse and longitudinal quadrupolar moments, respectively, by using the formulas as

$$M^z_{\frac{3}{2}} = \frac{1}{\beta Z}\frac{\partial Z}{\partial h_B}, \tag{11}$$

$$Q^x_{\frac{3}{2}} = \frac{1}{\beta Z}\frac{\partial Z}{\partial D_x}, \tag{12}$$

and

$$Q^z_{\frac{3}{2}} = \frac{1}{\beta Z}\frac{\partial Z}{\partial D_z}, \tag{13}$$

which are given explicitly as

$$\begin{aligned} M^z_{\frac{3}{2}} = \frac{1}{Z}\bigg[&-\exp\left(\frac{A_1}{2}\right)\cosh\left(\frac{C}{2}\right)-\exp\left(\frac{A_2}{2}\right)\cosh\left(\frac{C}{2}\right)\\ &+\exp\left(\frac{A_3}{2}\right)\cosh\left(\frac{E}{2}\right)+\exp\left(\frac{A_4}{2}\right)\cosh\left(\frac{E}{2}\right)\\ &-\left(\frac{2\beta(-D_x+2D_z-2h_B-2JzM^z_{\frac{1}{2}})}{C}\right)\exp\left(\frac{A_1}{2}\right)\sinh\left(\frac{C}{2}\right)\\ &-\left(\frac{2\beta(-D_x+2D_z-2h_B-2JzM^z_{\frac{1}{2}})}{C}\right)\exp\left(\frac{A_2}{2}\right)\sinh\left(\frac{C}{2}\right)\\ &-\left(\frac{2\beta(D_x-2D_z-2h_B-2JzM^z_{\frac{1}{2}})}{E}\right)\exp\left(\frac{A_3}{2}\right)\sinh\left(\frac{E}{2}\right)\\ &-\left(\frac{2\beta(D_x-2D_z-2h_B-2JzM^z_{\frac{1}{2}})}{E}\right)\exp\left(\frac{A_4}{2}\right)\sinh\left(\frac{E}{2}\right)\bigg], \end{aligned}$$

$$\begin{aligned} Q^x_{\frac{3}{2}} = \frac{1}{Z}\bigg[&\frac{5}{2}\exp\left(\frac{A_1}{2}\right)\cosh\left(\frac{C}{2}\right)+\frac{5}{2}\exp\left(\frac{A_2}{2}\right)\cosh\left(\frac{C}{2}\right)\\ &+\frac{5}{2}\exp\left(\frac{A_3}{2}\right)\cosh\left(\frac{E}{2}\right)+\frac{5}{2}\exp\left(\frac{A_4}{2}\right)\cosh\left(\frac{E}{2}\right) \end{aligned}$$

$$
\begin{aligned}
&- \left(\frac{\beta(2D_x + 2D_z - 2h_B - 2JzM^z_{\frac{1}{2}})}{C}\right) \exp\left(\frac{A_1}{2}\right) \sinh\left(\frac{C}{2}\right) \\
&- \left(\frac{\beta(2D_x + 2D_z - 2h_B - 2JzM^z_{\frac{1}{2}})}{C}\right) \exp\left(\frac{A_2}{2}\right) \sinh\left(\frac{C}{2}\right) \\
&+ \left(\frac{\beta(4D_x - 2D_z - 2h_B - 2JzM^z_{\frac{1}{2}})}{E}\right) \exp\left(\frac{A_3}{2}\right) \sinh\left(\frac{E}{2}\right) \\
&+ \left(\frac{\beta(4D_x - 2D_z - 2h_B - 2JzM^z_{\frac{1}{2}})}{E}\right) \exp\left(\frac{A_4}{2}\right) \sinh\left(\frac{E}{2}\right)\Bigg]
\end{aligned}
$$

and

$$
\begin{aligned}
Q^z_{\frac{3}{2}} = \frac{1}{Z}\Bigg[&\frac{5}{2}\exp\left(\frac{A_1}{2}\right)\cosh\left(\frac{C}{2}\right) + \frac{5}{2}\exp\left(\frac{A_2}{2}\right)\cosh\left(\frac{C}{2}\right) \\
&+ \frac{5}{2}\exp\left(\frac{A_3}{2}\right)\cosh\left(\frac{E}{2}\right) + \frac{5}{2}\exp\left(\frac{A_4}{2}\right)\cosh\left(\frac{E}{2}\right) \\
&+ \left(\frac{2\beta(-D_x + 2D_z - 2h_B - 2JzM^z_{\frac{1}{2}})}{C}\right) \exp\left(\frac{A_1}{2}\right) \sinh\left(\frac{C}{2}\right) \\
&+ \left(\frac{2\beta(-D_x + 2D_z - 2h_B - 2JzM^z_{\frac{1}{2}})}{C}\right) \exp\left(\frac{A_2}{2}\right) \sinh\left(\frac{C}{2}\right) \\
&- \left(\frac{2\beta(D_x - 2D_z - 2h_B - 2JzM^z_{\frac{1}{2}})}{E}\right) \exp\left(\frac{A_3}{2}\right) \sinh\left(\frac{E}{2}\right) \\
&- \left(2\frac{\beta(D_x - 2D_z - 2h_B - 2JzM^z_{\frac{1}{2}})}{E}\right) \exp\left(\frac{A_4}{2}\right) \sinh\left(\frac{E}{2}\right)\Bigg].
\end{aligned}
$$

In addition, one also needs the definitions of the net magnetization M_{net} and net quadrupolar moment Q_{net}, respectively, given as

$$M_{\text{net}} = |M^z_{\frac{1}{2}} - M^z_{\frac{3}{2}}| \tag{14}$$

and

$$Q_{\text{net}} = |Q^z_{\frac{3}{2}} - Q^x_{\frac{3}{2}}|. \tag{15}$$

The total magnetic susceptibility of the system is just the sum of the sublattice susceptibilities

$$\chi = \chi_A + \chi_B, \tag{16}$$

which can be calculated by using the definitions

$$\chi_A = \left(\frac{\partial M^z_{\frac{1}{2}}}{\partial h_A}\right)_{h_A=0} \tag{17}$$

and

$$\chi_B = \left(\frac{\partial M_{\frac{3}{2}}^z}{\partial h_B} \right)_{h_B=0}. \tag{18}$$

In Sec. 3, we illustrate the thermal variations of the order-parameters, net magnetization and quadrupole moment, and the susceptibility.

3. The Thermal Variations of Order-Parameters, Susceptibility and Compensation Properties

First, we have investigated the thermal behaviors of the order-parameters and the total magnetic susceptibility as indicated in different panels of Fig. 1 for given values of our model parameters. As seen, the sublattice magnetization with spin-$\frac{3}{2}$ shows three ground states (GSs) values, i.e. $\frac{1}{2}$, 1 and $\frac{3}{2}$, whereas the sublattice with spin-$\frac{1}{2}$ shows only one GS, i.e. $\frac{1}{2}$, as expected. Figure 1(a) obtained for $D_x/J = D_z/J = 0$ shows that $M_{\frac{1}{2}}^z$ and $M_{\frac{3}{2}}^z$ decrease continuously from their GS values ($\frac{1}{2}$ and $\frac{3}{2}$, respectively) with increasing temperature and finally vanish at the second-order phase transition temperature T_c. In addition, $Q_{\frac{3}{2}}^z$ and $Q_{\frac{3}{2}}^x$, respectively, decrease and increase with the temperature and then tend towards the asymptotic value of 1.25 as the temperature is increased for $T \gg T_c$. Figure 1(c) obtained for $D_x/J = 5$ and $D_z/J = 3.5$ illustrates that $M_{\frac{1}{2}}^z$ and $M_{\frac{3}{2}}^z$ start from their GS values ($\frac{1}{2}$ and 1, respectively) and they decrease continuously with temperature and go to zero at T_c. However, $Q_{\frac{3}{2}}^z$ and $Q_{\frac{3}{2}}^x$ start from 1.75 and they decrease with increasing temperature until T_c where their values become constant. The new GS $(\frac{1}{2}, 1)$ found at $T = 0$, resulting from the half mixed of $S_{jB}^z = \frac{3}{2}$ and $S_{jB}^z = \frac{1}{2}$ states on the sublattice B. A similar GS has been identified for this mixed-spin system in Fig. 2 of Ref. 29. Figure 1(e) calculated for $D_x/J = 0.0$ and $D_z/J = -6.0$ also presents a T_c. Indeed, the two sublattice magnetization curves after starting from the same GS value ($\frac{1}{2}$) decrease with the temperature and then vanish continuously at the T_c. Figures 1(b), 1(d) and 1(f) which express the thermal dependence of the total magnetic susceptibility (χ) are in perfect agreement with the order-parameter curves of Figs. 1(a), 1(c) and 1(e)), respectively. In fact, χ increases very rapidly until reaching a peak at the transition temperature and then decreases very rapidly as the temperature increases.

In Fig. 2, we illustrate the compensation properties encountered in this model. Thus, Figs. 2(a) and 2(b) are obtained for $D_x/J = 1$ and $D_z/J = -0.75$. In Fig. 2(a), as the temperature increases, $M_{\frac{1}{2}}^z$ increases first from its saturation value and then decreases until vanishes at the T_c whereas $M_{\frac{3}{2}}^z$ decreases continuously and go to zero at the same T_c. The sublattice magnetizations $M_{\frac{1}{2}}^z$ and $M_{\frac{3}{2}}^z$ curves cross each other at the compensation temperature $T_{\mathrm{comp},M}$. Figure 2(b) shows that the net magnetization curve also goes to zero at $T_{\mathrm{comp},M}$ first and then at T_c. Figures 2(c) and 2(d) are calculated for $D_x/J = 1$ and $D_z/J = 0$. In Fig. 2(c), $Q_{\frac{3}{2}}^z$

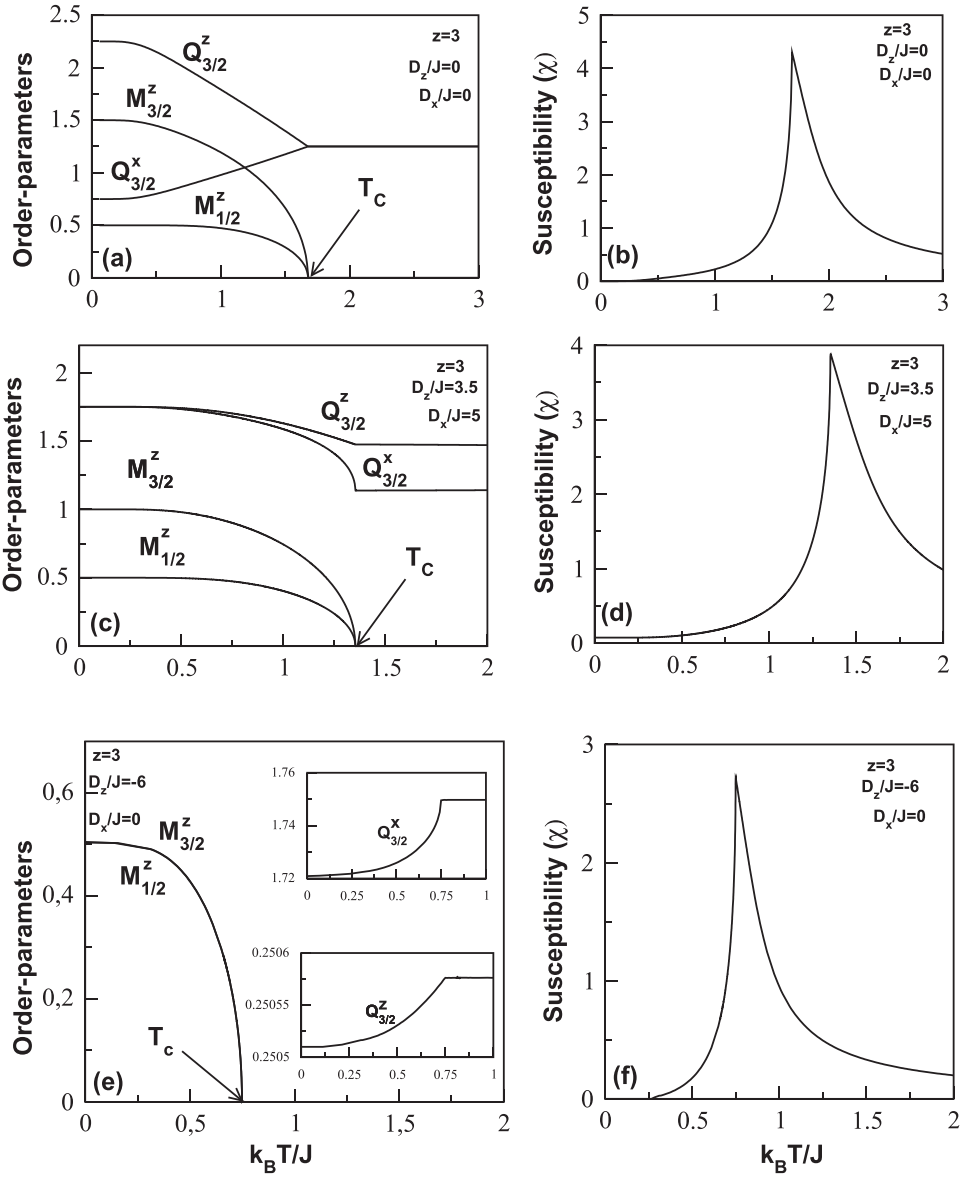

Fig. 1. Thermal behaviors of the order-parameters and the total magnetic susceptibility in the absence of external magnetic field for given values of model parameters reported in different panels. T_c indicates the second-order phase transition temperature.

and $Q^x_{\frac{3}{2}}$ have the same behavior as in Fig. 1(a) but now the quadrupole moment curves cross each other at the compensation temperature $T_{\mathrm{comp},Q} < T_c$. A similar behavior was also observed in Fig. 2 of Ref. 31 and Fig. 1(d) of Ref. 19. The thermal behavior of the net quadrupole moment depicted in Fig. 2(d) shows that the net quadrupole moment Q_{net} also goes to zero at the $T_{\mathrm{comp},Q}$. It is important to indicate

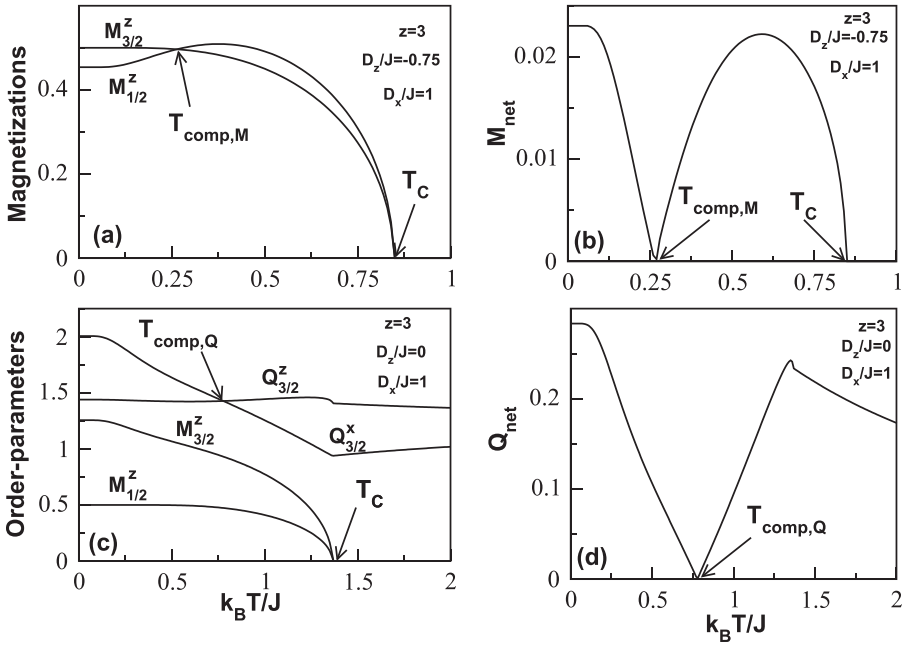

Fig. 2. Thermal behaviors of the order parameters, $M_{\rm net}$ and $Q_{\rm net}$ in the absence of external magnetic field for given values of model parameters reported in different panels. The model exhibits two special compensation temperatures denoted by $T_{{\rm comp},M}$ and $T_{{\rm comp},Q}$, respectively.

that the $T_{{\rm comp},M}$ and $T_{{\rm comp},Q}$ lines existing in the model for possible values of D_x and D_z are displayed in the different phase diagrams in Sec. 4.

After having completed the thermal variations of our thermodynamic parameters, we are now ready to obtain the phase diagrams in the next section.

4. The Thermal Phase Diagrams

The thermal behaviors of the order-parameters allow us to calculate the phase diagrams on the $(D_z/J, k_BT/J)$ and $(D_x/J, k_BT/J)$ planes for $h_A = h_B = 0$. In these phase diagrams, the T_c-, $T_{{\rm comp},M}$- and $T_{{\rm comp},Q}$-lines are indicated with the solid, dashed and dotted-dashed lines, respectively.

The first phase diagrams plotted in Fig. 3 are obtained on the $(D_z/J, k_BT/J)$ planes for $z = 3, 4, 6$ and $D_x = 0$ which corresponds to the Blume–Capel model. In this case, the model yields only the T_c-lines. In addition, the $T_{{\rm comp},Q}$-lines can be observed for all z. All the transition lines are seen at higher temperatures for higher $z's$. As seen, the $T_{{\rm comp},Q}$-lines which start from their corresponding T_c-lines and terminate at $k_BT/J = 0$ are seen in the region with negative values of D_z. The quadrupolar moments Q_x and Q_z compensate each other. For large negative/positive values of D_z, the critical temperatures tend towards a constant value which is smaller for large negative values than for large positive values. This

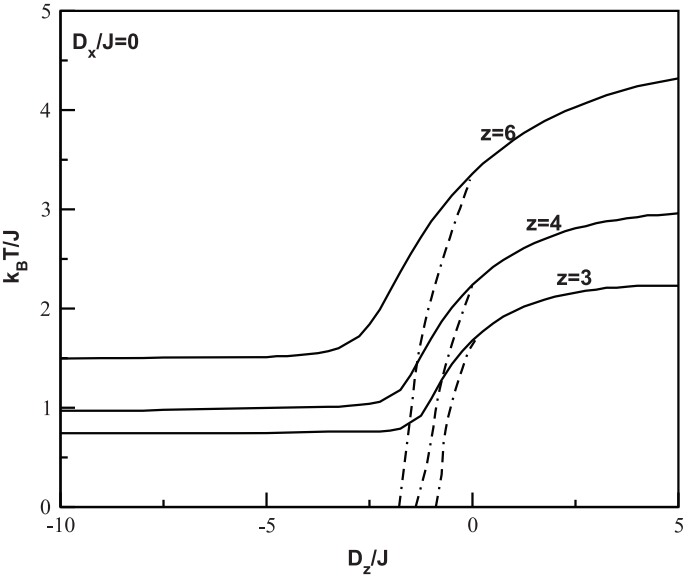

Fig. 3. Phase diagrams on the $(D_z/J, k_BT/J)$ planes for $D_x/J = 0$ when $z = 3, 4, 6$. Solid lines denote the second-order transitions lines, i.e. T_c-lines while dotted-dashed lines represent $T_{\mathrm{comp},Q}$ compensation lines.

is attributed to the fact that in the system only the GS's $[\pm\frac{1}{2}, \pm\frac{1}{2}]$ and $[\pm\frac{3}{2}, \pm\frac{1}{2}]$ exist, respectively, for large negative/positive values of D_z. For the intermediate values, the transition temperature increases as a function of D_z. This behavior was also observed in some other works. In fact, in Fig. 1, of Ref. 29, the same model is investigated by means of the Oguchi approximation similar trends, which are found. Our findings can also be compared to those obtained from the studies of the mixed spin-$\frac{1}{2}$ and spin-$\frac{3}{2}$ Blume–Capel model using the ERR calculations on the Bethe lattice and on the Cayley tree,[32,33] and with the EFT,[34] as a result, perfect agreements are obtained. In addition, the phase transition temperatures are found to be at $k_BT/J = 0.7439, 0.9699, 1.4230$ corresponding to $z = 3, 4$ and 6, respectively, for large negative values of D_z. When these values are compared to those calculated in the previous works, one remarks that our approach overestimates the transition temperatures, which is also seen in the Oguchi approximations.[29] So, it is the result of the used method and thus the model needs improvement.

The next phase diagrams displayed in Fig. 4 are calculated on $(D_z/J, k_BT/J)$ planes for $z = 3$ and with positive/negative values of D_x. Figure 4(a) calculated for negative D_x indicates that this mixed-spin system yields only T_c-lines and the $T_{\mathrm{comp},M}$-lines which emerge from their corresponding T_c-lines and terminate at $k_BT/J = 0$ as before. The T_c-lines start from a constant value for large negative D_z values and then decrease with increasing the temperature until reaching a minimum from where they increase to finally tending towards an asymptotic value for large

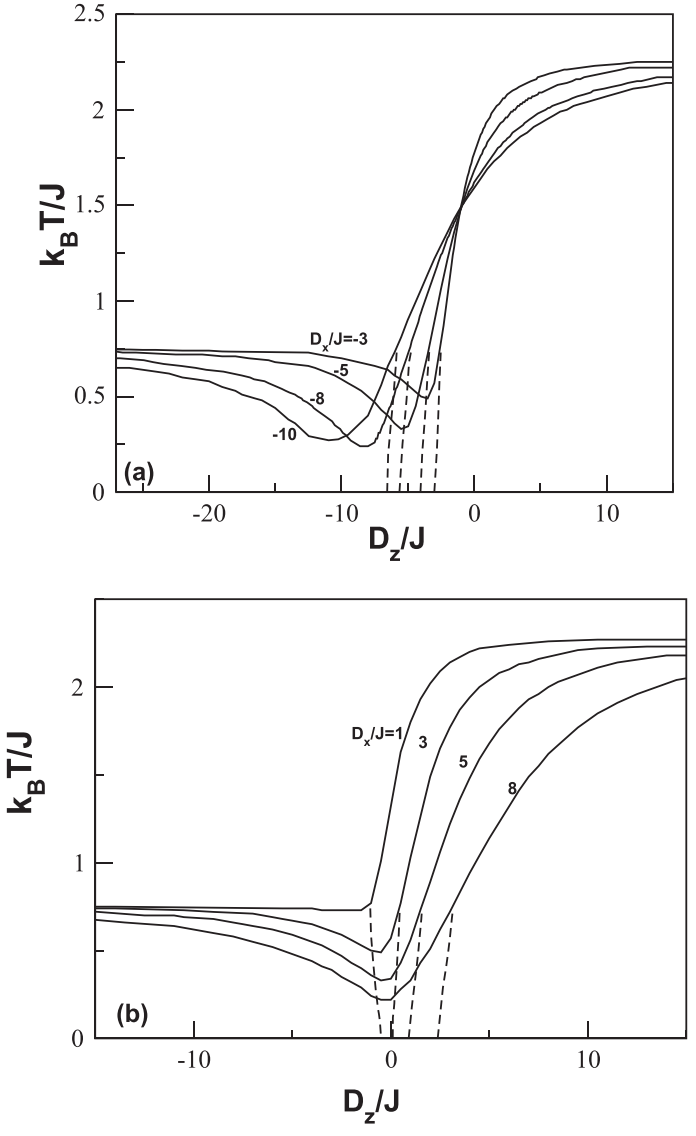

Fig. 4. Phase diagrams on the $(D_z/J, k_BT/J)$ planes for $D_x/J \neq 0$ when $z = 3$. Solid lines denote the second-order transitions lines, i.e. T_c-lines while dashed lines represent $T_{\mathrm{comp},M}$ compensation lines.

positive D_z values. All the transition lines intersect at $D_z = -1$. The case of positive values of D_x is plotted in Fig. 4(b). It is also found that the system exhibits only the T_c-lines. The $T_{\mathrm{comp},M}$-lines are also observed. The shapes of transition lines are similar to those of Fig. 4(a) except that these lines do not intersect.

The last phase diagrams are displayed on the $(D_x/J, k_BT/J)$ planes for $z = 3$ and for given values of Dz, as shown in Fig. 5. In Fig. 5(a), we see that for

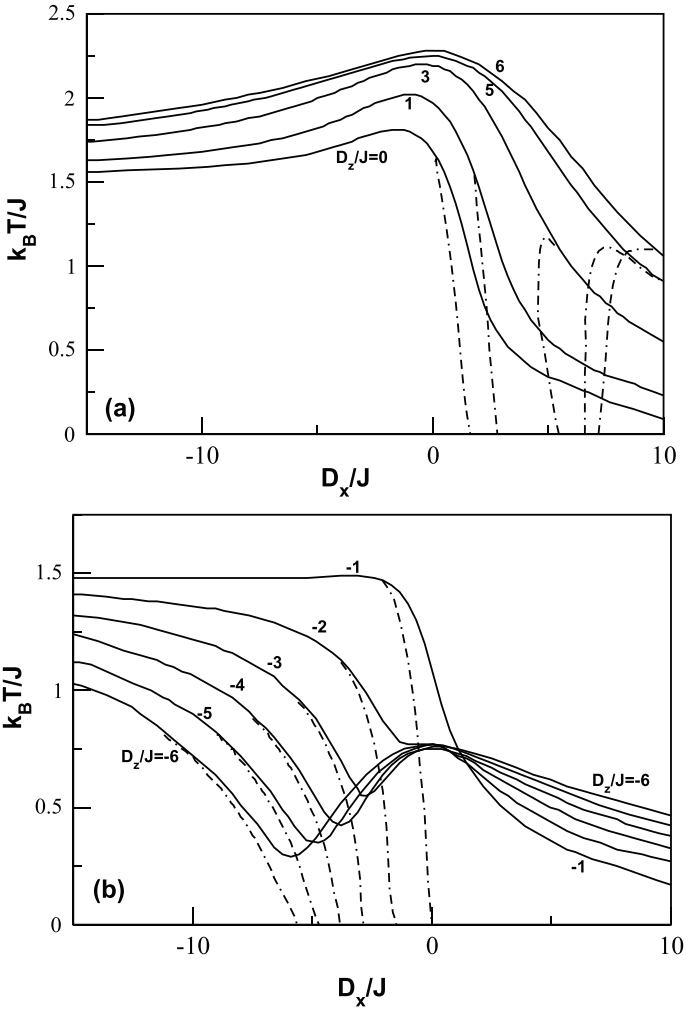

Fig. 5. Phase diagrams on the $(D_x/J, k_BT/J)$ planes for given D_z/J when $z = 3$. Solid lines denote the second-order transitions lines, i.e. T_c-lines while dotted-dashed lines represent $T_{\mathrm{comp},Q}$ compensation lines.

$D_z/J = 0, 1, 3, 5$ and 6, the T_c-lines start from higher temperatures, increase with D_x and reach peaks before decreasing towards lower temperature values. As D_z/J increases, the transition temperature increases and the peak shifts to the right. The $T_{\mathrm{comp},Q}$-lines are found for $D_x > 0$. Figure 5(b) obtained for $D_z/J = -1, -2, -3, -4, -5$, and -6, indicates that for $D_z/J < -1$, the T_c-lines start from higher temperature, decrease with D_x and reach a minimum from where they increase to go towards a greater value and then they decrease again then tend towards the lower temperatures values. The $T_{\mathrm{comp},Q}$ lines are found for $D_x < 0$.

5. Conclusion

In this work, we have studied the magnetic properties and phase diagrams of the mixed spin-$\frac{1}{2}$ and spin-$\frac{3}{2}$ Ising–Heisenberg model by using a new approach of the MFA. By investigating the thermal behaviors of our model, we were able to detect the presence of different phases at $T = 0$ and to calculate the phase diagrams on the $(D_z/J, k_BT/J)$ and $(D_x/J, k_BT/J)$ planes. According to the values of Hamiltonian interaction parameters, our model exhibits the second-order phase transitions and also two different compensation behaviors. The phase diagrams obtained when the model is reduced to the Blume–Capel model are qualitatively similar to those found in the literature. However, we should note that this new approach overestimates the transition temperatures[29] and needs to be improved. The compensation obtained for the magnetizations has many applications in science and technology, but the compensation for the quadrupole moments was first pointed out in Ref. 19 and its possible applications need to be searched further.

References

1. A. Maritan, M. Cieplak, M. R. Swift, F. Toigo and J. R. Banavar, *Phys. Rev. Lett.* **69** (1992) 221.
2. J. M. Manriquez, G. T. Yee, R. S. Mclean, J. A. Epstein and J. S. Miller, *Science* **252** (1991) 1415; B. G. Morin, P. Zhou, C. Hahm and J. A. Epstein, *J. Appl. Phys.* **73** (1991) 5648.
3. C. Ekiz, J. Strečka and M. Jaščur, *J. Magn. Magn. Mater.* **323** (2011) 493.
4. S. Lyan and C. Z. Yang, *Phys. Stat. Sol. (b)* **208** (1998) 151.
5. S. Lackova, M. Jaščur and T. Horiguchi, *Physica A* **339** (2004) 416.
6. N. Benayad and R. Zerhouni, *Phys. Stat. Sol. (b)* **201** (1997) 491.
7. J. Strečka, L. Canová and K. Minami, *Am. Inst. Phys.* **1198** (2009) 156.
8. L. Canová, J. Strečka and M. Jaščur, *Czech. J. Phys.* **54** (2004) D579.
9. H. Wu, G. Wei, P. Zhang, G. Yi and W. Gong, *J. Magn. Magn. Mater.* **322** (2010) 3502.
10. J. Strečka and M. Jaščur, *J. Phys. Condens. Matter* **15** (2003) 4519.
11. W. Jiang, G. B. Xiao, G. Z. Wei, A. Du and Q. Zhang, *Commun. Theor. Phys.* **41** (2004) 131.
12. Y. Belmamoun and M. Kerouad, *Phys. Scr.* **77** (2008) 025706.
13. M. Boughrara and M. Kerouad, *Physica A* **374** (2007) 669.
14. K. Htoutou, A. Ainane and M. Saber, *J. Magn. Magn. Mater.* **269** (2004) 245.
15. W. Jiang, G. Z. Wei and A. Du, *J. Magn. Magn. Mater.* **250** (2002) 49.
16. C. Q. Xu and S. L. Yan, *J. Magn. Magn. Mater.* **416** (2016) 48.
17. C. Q. Xu and S. L. Yan, *J. Magn. Magn. Mater.* **345** (2013) 261.
18. H. Wu, G. Wei, P. Zhang, G. Yi and W. Gong, *J. Magn. Magn. Mater.* **322** (2010) 3502.
19. E. Albayrak, *Chin. Phys. Lett.* **35** (2018) 037501.
20. B. Deviren, M. Keskin and O. Canko, *J. Magn. Magn. Mater* **321** (2009) 458.
21. A. Bobák and M. Jurčišin, *J. Phys. IV France* **07** (1997) C1-179.
22. N. Benayad, A. Dakhama, A. Klmper and J. Zittartz, *Ann. Phys.* **5** (1996) 387.
23. N. Benayad, A. Dakhama, A. Klmper and J. Zittartz, *Z. Phys. B* **101** (1996) 623.
24. G. M. Buendia and R. Cardona, *Phys. Rev. B* **59** (1999) 10.

25. J. Li, G. Wei and A. Du, *J. Magn. Magn. Mater.* **269** (2004) 410.
26. C. Ekiz, *J. Magn. Mater.* **293** (2005) 913.
27. X. Zhang and X.-M. Kong, *Physica A* **369** (2006) 589.
28. M. Jaščur and J. Strečka, *Physica A* **358** (2005) 393.
29. A. Bobák, Z. Fecková and M. Žukoviǩ, *J. Magn. Magn. Mater* **323** (2011) 813.
30. W. Qin, H. Yin, P. Zhang, Z. Wang and X. King, *J. Supercond. Nov. Magn* **34** (2021) 963.
31. N. C. Eddeqaqi, M. Saber, A. El-Atri and M. Kerouad, *Physica A* **272** (1999) 144.
32. E. Albayrak, *Mod. Phys. Lett. B* **32** (2018) 1850325.
33. E. Albayrak and A. Alçi, *Physica A* **345** (2005) 48.
34. W. Jiang, G. Wei and Z. Xin, *Physica A* **293** (2001) 455.